Journal of Fluid Science and Technology

Vol. 4, No. 2, 2009

Control of Flow and Heat Transfer Characteristics in an Impinging Jet with Acoustic Excitation*

Shouichiro IIO**, Yoshiaki HANEDA***, Yasumitsu MATSUBARA** and Toshihiko IKEDA**

**Department of Environmental Science and Technology, Shinshu University, 4-17-1 Wakasato, Nagano 380-8553, Japan.
E-mail: shouiio@shinshu-u.ac.jp

**Department of Mechanical Engineering, Nagano National College of Technology, 716 Tokuma, Nagano 381-8550, Japan.

Abstract

The experimental study of flow field and heat transfer characteristics of a submerged, rectangular jet impinging normally on a flat plate is presented. Four nozzle-to-surface spacing of H/w=3, 6, 10 and 20 with acoustic excitations was performed experimentally. The forcing Strouhal number is set from St=0.1 to 0.9 at 0.1 intervals. Velocity distributions with two excitation modes, symmetric and asymmetric excitation, are investigated by means of hot-wire measurement. It was found that the basic flow fields changed drastically, while there is little difference of heat transfer characteristic for both the excitation modes. For the short nozzle-to-plate distances, the heat transfer was enhanced in the wall jet region for the excitation of St=0.2. The maximum heat transfer ratio was obtained at the stagnation point for the middle spacing of H/w=6 for St=0.5. It was revealed that the non-periodic velocity component played the most important role in promotion of the heat transfer with acoustic excited impinging jet.

Key words: Impinging Jet, Heat Transfer, Acoustic Excitation, Velocity Decomposition

1. Introduction

Impinging jet heat transfer has been used in a wide range of industrial applications. A relatively small issuing power for impinging jets makes fine adjustment of the heat transfer coefficient easily by controlling the flow rate. Several technologies for controlling impinging jet heat transfer have been developed to further improve efficiency, and to conserve energy for a variety of applications using impinging jets.

Gardon and Akfirat[1,2] studied the effects of impingement distance, Reynolds number, and free-stream turbulence on the characteristics of heat transfer for a plane impinging jet and an axisymmetric impinging jet. Oyakawa et al.[3] investigated the characteristics of impingement jet heat transfer using a cross-shaped nozzle. These researchers found that the potential core length of the jet was extended, and that the high heat transfer coefficient at the stagnation point was kept downstream, and they revealed the mechanisms of these phenomena. Hiwada et al.[4] investigated the effect of the width, length and number of tabs at the nozzle exit on the heat transfer characteristics of an axisymmetric impinging air jet. When two tabs were positioned at the exit of a circular nozzle, the heat transfer characteristics changed significantly with flattened distribution profiles of the heat transfer

*Received 14 Nov., 2008 (No. 08-0804)
[DOI: 10.1299/jfst.4.304]

coefficients. In addition, Haneda et al.[5] demonstrated that the self-vibrating cylinder elastically suspended into the jet impingement region enhanced heat transfer.

An increasing number of reports on heat transfer control using acoustic wave excitation have been published lately. Liu and Sullivan[6] investigated the influence of excitation frequency on local flow structures and heat transfer in the wall-jet region for an axisymmetric impinging jet. Enhancement and reduction of local heat transfer in the wall-jet region can be attained by forcing the impinging jet near the natural frequency and its subharmonic frequency, respectively.

An experimental study was conducted by Hwang et al.[7] to investigate the relationship between acoustic excitation positions and the heat transfer characteristics for an axisymmetric impinging jet. The heat transfer characteristics showed a dramatic change when acoustic excitation was applied to a shear layer. Excitation by a natural vortex-shedding frequency resulted in a shortened potential core length, increased turbulence intensity at the upstream region, and a reduction in the nozzle-to-plate distance in which the maximal heat transfer coefficient was obtained. Edmund et al.[8] investigated the heat transfer characteristics of two-dimensional impinging air jet by changing the Reynolds number and the nozzle-to-plate distance when the flow was excited using an acoustic disturbance with 10% of the velocity fluctuation to the mean velocity of the free jet. When an impingement plate was positioned at eight times downstream of the nozzle width from the jet exit, the heat transfer coefficient was 57 % increased at the stagnation point by the excitation of natural vortex-shedding frequency. Experiments were performed by Gau et al.[9] to study heat transfer when the jet shear layer was acoustically excited using a subharmonic or nonharmonic frequency. Excitations at the subharmonic frequency greatly enhanced heat transfer, while heat transfer decreased at a nonharmonic frequency. In the previous paper[10] we focused on the control technique related to edge-tone in the jet-wedge system using acoustic excitation. It was reveled the effect of the excitation phase pattern on the sound pressure level of the edge-tone.

The purpose of the present study is to investigate the flow and heat transfer characteristics of the acoustic excited jet by changing the excitation frequency and mode. This investigation deals with the velocity fields of free jet, and with the heat transfer on the impinging plate by changing the nozzle-to-plate distance.

2. Experimental apparatus and procedure

A schematic illustration of an experimental set-up is shown in Fig.1. The test section including a wind tunnel and a nozzle are set in the sound proof chamber to attenuate perturbations such as noises from outside. Dimensions of the chamber are 2.0 m in height, 1.8 m in width and 2.7 m in length. The inner wall of the chamber is covered with glass wool mat of 50 mm thickness except for the floor. The ceiling of the chamber has a socket to mount of a wind tunnel consist of a silent duct, flow-rectifying device such as a honeycomb and wire screens. A contraction nozzle is mounted of the wind tunnel exit. The side wall has exhaust opening to connect through a silent duct to a blower setting outside. The blower generates negative pressure by sucking up air in the chamber, then the jet issues from the nozzle exit. The jet velocity is regulated with variable speed motor attached to the blower. The detailed around the test section is shown in Fig. 2. The coordinate system is fixed at the nozzle center, the origin is located at the center of the jet exit, the x-axis is along the flow direction, the y-axis is in the horizontal direction perpendicular to the flow, and the z-axis is in the spanwise direction of the nozzle. The tunnel has a rectangular cross section nozzle. The dimensions of the nozzle are 10 mm in width, w, 150 mm in length, h, the aspect ratio (h/w) of 15, and the contraction ratio is 10.0. A honeycomb and fine screens are installed in the tunnel for further managing the flow quality. The flow velocity at the origin was set equal to U_0=10 m/s which correspond to Reynolds number ($Re = U_0 w/ \nu$) of 6700,

where ν is a kinematic viscosity of air. The flow velocity at the nozzle exit, U_0, is calculated from the measured pressure drop across the nozzle. The flow temperature is kept constant by the air conditioner and the ceiling fan in the room. The acoustic disturbance is inserted from a pair of slot devices which is set at the nozzle exit, it is therefore possible to impose either symmetric or asymmetric excitation on the jet. The each acoustic disturbance from two slot devices has no phase lag for the symmetric excitation, and is opposite phase for the asymmetric excitation. The excitation amplitude is defined as u_{prms} that the root mean square value of fluctuating velocity at the slot exit. u_{prms}/U_0 is set at 2.0 %. It is note that the streamwise turbulence intensity at the nozzle exit without excitation was about 0.4 % of U_0=10 m/s. The excitation frequency, f_p, was set from 100 to 900 Hz at 100 Hz interval, the fundamental frequency of the non-excited jet flow was 300 Hz. The detail of the slot is shown in a blow up in Fig. 2. The opening gap of slot tip is 0.5 mm and the slot meets the nozzle exit plane at an angle of 30°. The slot device is shown in Fig. 3. The slot is partitioned into eight cells by thin Plexiglas plates as shown in Fig. 3, it is also possible to impose zigzag excitation (see Fig. 8). Each cell is connected to loudspeaker with vinyl pipes having an inner diameter of 9.5 mm. The power of the loudspeakers used for control is 300 watts and the diameter is 300 mm.

Local surface temperature or heat transfer coefficients on the impingement surface are measured by the thermocouples under a constant heat flux condition. The nine stainless steel strips 20 μm thick and 15 mm wide were glued in parallel with each other on the impingement surface. They were electrically connected in series and were heated by passing alternating electric current. The electric current is controlled by a variable power supply and measured precisely using a current sensor within ±1.0 %. Distributions of the heated surface temperature was measured with 57 thermocouples allocated to contact with the back surface of the central strip at 4 mm interval so as to cover between $-6<y/w<6$, and at 5mm interval between $-12.5<y/w<-6$, $6<y/w<12.5$.

The local Nusselt number, Nu, was defined by $Nu=qw/\lambda(T_w-T_0)$, where λ is the thermal

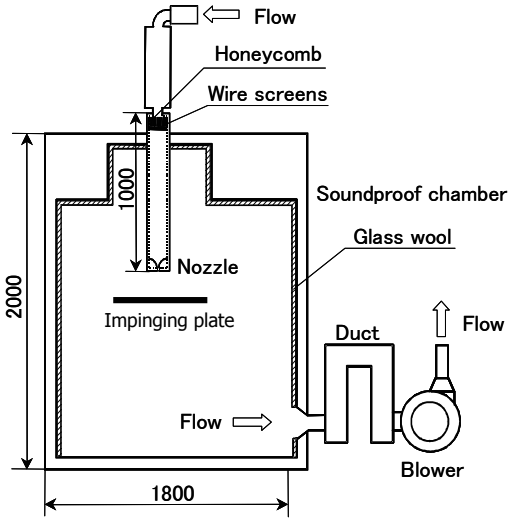

Fig. 1 Experimental apparatus

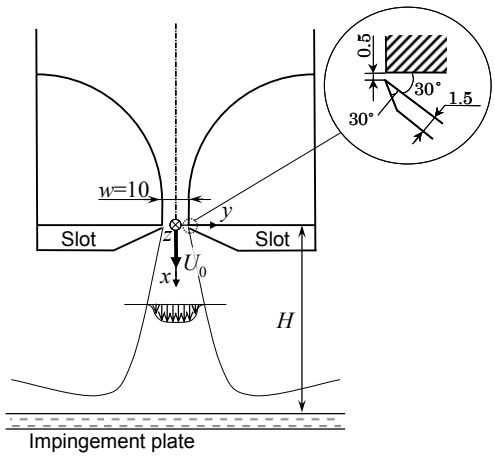

Fig. 2 Test section

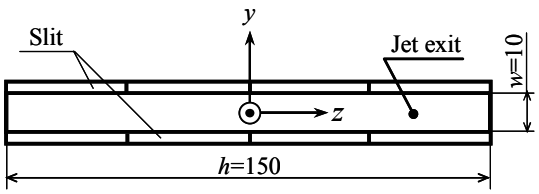

Fig. 3 Slot device for acoustic excitation

conductivity of the jet air, T_w is a local surface temperature, T_0 is the jet temperature and q is a heat flux from the surface. The strouhal number, St, indicates the frequency characteristics of the flow and is defined by $St=f_p w/U_0$, where f_p is the excitation frequency, $St=0$ means the non-excitation condition in this study.

The velocity measurement was performed by using a constant temperature anemometer that consisted of a 2.5 μm platinum wire with a length of 1 mm. The hot wire is calibrated by a high-precision pressure transducer and Pitot-tube measurements according to the King's law. A 16-bit A/D converter is connected to a personal computer for data acquisition. The probe is inserted into the flow downstream position by a handmade support without disturbing the flow. The sensing probe is facilitated by a three-dimensional traversing system that is driven by stepping motors under the personal computer control.

3. Phase average technique

The eduction of the coherent structure as well as interpretation of the data requires introduction of the concept of phase average[8]. In this experiment we used the cyclic position of the speaker signal as a clock for selective sampling, which permitted us to extract the organized wave motion from a background field of finite turbulent fluctuations. We decomposed the fluctuating velocity $u(x, t)$ as

$$u(x,t) = U(x) + \tilde{u}(x,t) + \hat{u}(x,t)\,; \tag{1}$$

U is the streamwise mean velocity, $\tilde{u}$ is the periodic (phase average) velocity and $\hat{u}$ is the turbulence (non-periodic velocity). We also use the definition of the phase average velocity at a particular time θ in the period T of the periodic perturbation, then

$$\tilde{u}(x,\theta) = \lim_{N\to\infty} \frac{1}{N} \sum_{n=1}^{N} \{ u(x,\theta+nT) - U(x) \}. \tag{2}$$

The difference between the instantaneous signal and the phase average represents the background random fluctuation, and the difference between the phase average and the time average denotes the (periodic) coherent component. Thus, knowing the period of the induced perturbation, the mean, coherent and random components of the velocity signal can be extracted from the instantaneous total velocity signal.

4. Results and discussion

4.1. Flow characteristics

To investigate the relationship between the velocity field and the excitation condition (frequency, mode), the streamwise velocity distribution along the jet axis without the impinging plate is shown in Fig. 4. For the non-excited jet, the potential core region is observed $x/w<5$, then the velocity decays slightly from $x/w=5$, and decreased monotonically in the downstream region over $x/w=8$. This centerline velocity was proportional to minus one-half power of the x. Figure 4(a) shows the centerline velocity for the asymmetric excitation. The potential core region shortens with excitation. For $St=0.4$, it is much differ from the non-excited jet. The mean velocity decays from $x/w=4$, and shows an initial decline followed by a slight rise with increasing the streamwise position. After the slight rise, the velocity decreases gradually for $x/w>8$. For the excited St of 0.6 and 0.8, the potential core shortens but the slope does not change. For the symmetric excitation jet as shown in Fig. 4(b), the potential core region became shorter with excitation. For the excited St of 0.2, it can be observed that the velocity decreases upstream, then the velocity decaying decelerates over $x/w=10$.

The streamwise growth of the fluctuating velocity along the jet centerline is plotted in Fig. 5. Solid marks show RMS value of the periodic velocity, $\tilde{u}_{rms}$, and open marks show RMS value of the non-periodic velocity, $\hat{u}_{rms}$. The solid line is turbulence intensity, u'_{rms}, which includes of the periodic velocity, since the velocity decomposition could not apply

for the non-excited jet. For both excitation modes as shown in Figs. 5(a) and (b), the u'_{rms} increases exponentially up to x/w=4, and slightly increases up to x/w=10, and then monotonically decreases at the downstream region. For the asymmetric excitation as shown in Fig. 5(a), the growth of $\tilde{u}_{rms}$ starts later with the value of St is smaller, and the maximum value of $\tilde{u}_{rms}$ is larger. For the excited St of 0.2 and 0.4, in the downstream region, the value of $\tilde{u}_{rms}$ was relatively large compared with that the other excitation conditions. For St=0.2, the distribution of $\hat{u}_{rms}$ partly corresponded with that of u'_{rms} for St=0.0. As the value of St increasing, $\hat{u}_{rms}$ grew rapidly compared to the non-excited jet. For symmetric excitation (Fig. 5(b)), the value of $\tilde{u}_{rms}$ monotonically decreases for $St\geq0.4$, but the tendency changes substantially for St=0.2, $\tilde{u}_{rms}$ increases up to x/w=5, then rapidly decreases. In contrast, values of $\hat{u}_{rms}$ for $St\geq0.4$ are higher than that for St=0.2.

The velocity distributions depend on the excitation pattern and frequency as shown in Figs. 4 and 5. We, therefore, conducted the flow visualization with smoke method, not shown here, to clarify the difference of vortex structure with the excitation conditions. The observation result exhibited the vortex arrangement subsequent to the varicose mode growth for the symmetric excitation or the sinusoidal mode growth for the asymmetric excitation. Then, the vortices became larger and clearer with decreasing the excitation Strouhal number for $St\leq0.4$. In contrast, the difference of vortex arrangement became unclear for $St>0.6$ in the both excitation modes. The reason for the difference of the velocity distributions for $St\leq0.4$ with both the excitation modes is the change of the vortex formation. We suggest from our observations that the excitation conditions may also correlate strongly with heat transfer characteristics.

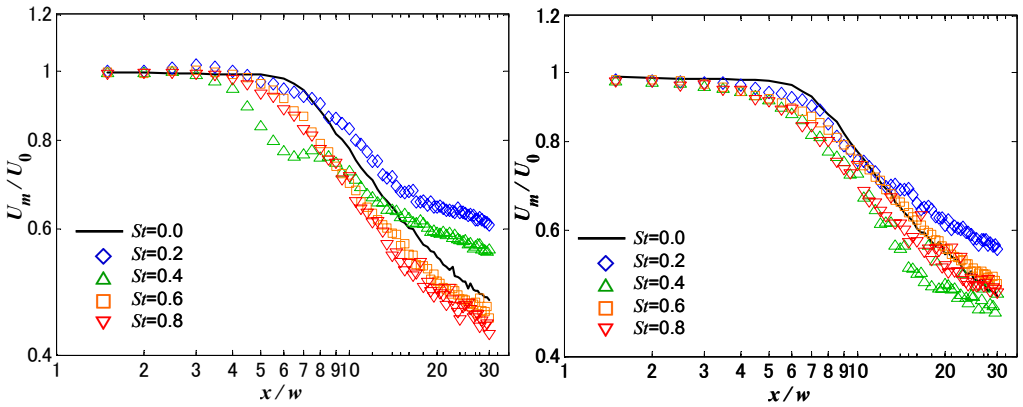

(a) Asymmetric excitation (b) Symmetric excitation

Fig. 4 Mean streamwise velocity distribution on the x-axis

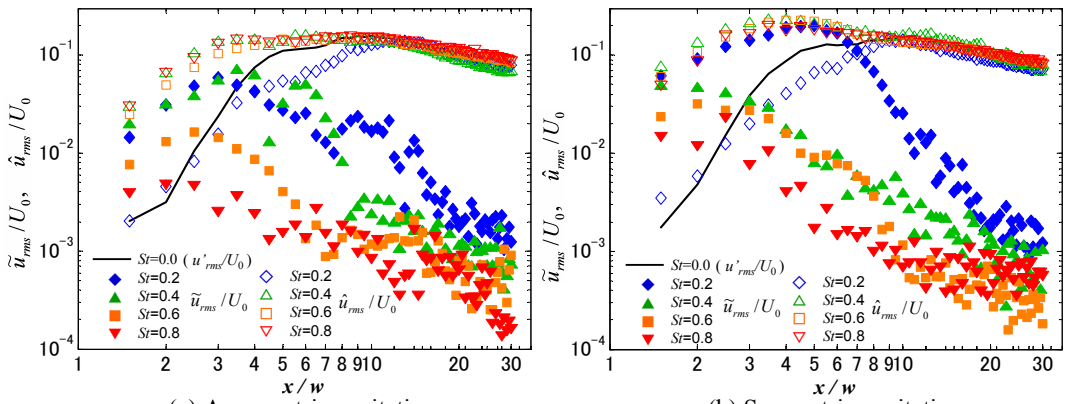

(a) Asymmetric excitation (b) Symmetric excitation

Fig. 5 Fluctuating velocity distribution on the x-axis

4.2. Heat transfer characteristics

Figure 6 shows the effects of H/w and St on Nusselt number at a stagnation point. For the case of non-excited jet, the Nusselt number gradually increases with increasing the nozzle-to-plate spacing, and then a peak appears at H/w=8. As the gap distance increases (H/w>8), the Nu value decreases. The variation of Nusselt number is in accord with the results by Kumada et al.[12]. For the asymmetric excited jets shown as Fig. 6(a), the local heat transfer is enhanced in the range of 4≤H/w≤6, but is suppressed for the gap distance of H/w≥8. The distribution pattern of Nu value is complicated for the excited St of 0.1 and 0.2. For St≥0.5, the distribution patterns are similar and Nu has a peak at H/w=7. The peak values are higher than that of the non-excited jet, but are lower for St≤0.4. The peak position shifts upstream with the acoustic excitation, this tendency is same the results reported by Hwang et al.[7]. Maximum enhancement ratio of local Nusselt number achieved here is about 17 % for St=0.2 at H/w=5. For the symmetric excited jet except in St=0.1, the Nusselt

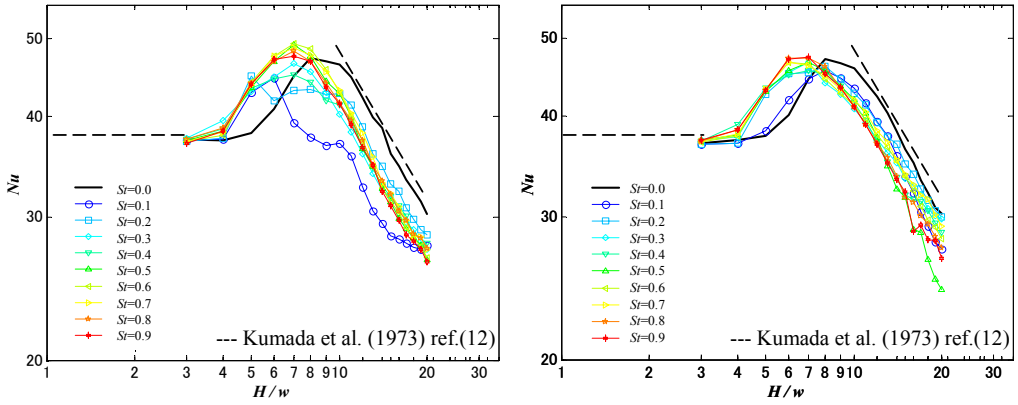

(a) Asymmetric excitation (b) Symmetric excitation

Fig. 6 Effects of H/w and St on Nu at stagnation point

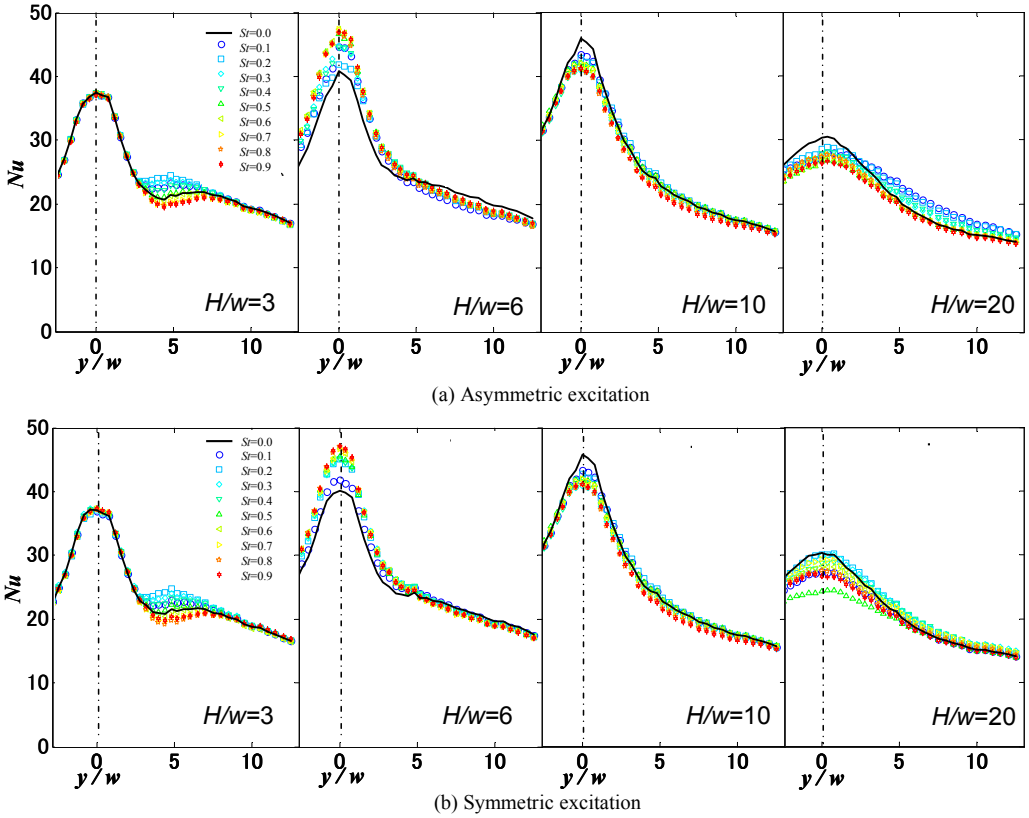

(a) Asymmetric excitation

(b) Symmetric excitation

Fig. 7 Effects of H/w and St on Nu distribution

number at the gap distance of $H/w \leq 6$ is higher than that of the non-excited jet and the position of the peak shifts upstream. At the large gap distance of $H/w \geq 8$, the Nusselt numbers in any excitation frequencies are lower than that of the non-excited jet. For both excitation modes, there is no clear connection between the distribution of *Nu* and the velocity distributions.

We conducted visualization of the vortex structure by smoke method, not shown here, to clarify the difference between the both *Nu* distributions shown in Figs. 6 (a) and (b) for the excitation of St=0.1, 0.2. The observation result showed that the vortex for the asymmetric excitation is larger than that for the symmetric excitation. For asymmetric excitation, enlarged vortex structures enhanced the jet diffusion, then, the jet center velocity decayed rapidly, for this reason it is surmised that the heat transfer rate was suppressed as shown in Fig. 6(a). In contrast, for the symmetric excitation, the vortex enlargement did not observe by decreasing the Strouhal number from 0.4, it is unknown why the heat transfer rate was not enhanced for the excitation of St=0.1. Further experimental work is needed in this respect.

Figure 7 presents the effects of H/w and St on the minor axis distribution of the *Nu* value. For H/w=3, 6 and 10, same distribution patterns are observed in both the excitation modes. For a small gap (H/w=3), there are two types of peak in Nusselt number. The first peak appears at the stagnation point. The secondary peaks appear at $y/w \approx \pm 5$. Gardon et al.[1] proposed that the secondary peak in the Nusselt number is induced with the transition from laminar to turbulent boundary layers. This transition was aided by the increasing turbulence level in a main stream. The position of the second peak moves slightly inward in the nozzle width direction owing to the enhancement of the flow transition with the low frequency excitation. For the excited St of 0.2, the maximum peak value is obtained at y/w=5. As the gap distance increases at $H/w \geq 6$, there is only one peak at the stagnation region. At the medium gap distance of H/w=6, Nusselt number is sufficiently higher than that of the non-excited jet around the stagnation region. It is because the excited jet flow has relatively high turbulence intensity. At the large gap distances of H/w=10 and 20, the *Nu* value increases slightly in outer region with asymmetric excitations shown as Fig. 7(a). In contrast, the enhancement of the heat transfer rate is not observed with symmetric excitations as shown in Fig. 7(b). This difference is most likely due to a spreading of the jet with asymmetric excitation.

Although it was found that the velocity distribution was quite different with the excitation mode and frequency, there is little difference of *Nu* distributions as shown in Fig. 7. Next, we tried the zigzag excitation as shown in Fig. 8 to clarify the most important velocity component which enhances the heat transfer. In Fig. 8, the same phase excitation irradiated through the same colored cell, both the excitations with the blue colored cell and with the red colored one is opposite in phase. Section A, B, and C illustrated as dashed line is boundary part of the each cell. Iio et al.[10] reported that the zigzag excitation induced sinusoidal deformation of the jet in the yz-plane from a rectangular nozzle. The wavelength of the deformation was approximately equal to the cell length in the z-direction near the nozzle of x/w<5, and the wave nodes were corresponded to the each boundary part of the cells. The alternative oscillation was occurred at the both sides of node (boundary part), hence the fluctuating velocity component was increased near the node. Taking the experimental result mentioned above into consideration, the heat transfer rate could be influenced near the node. From the result of velocity measurement shown in Fig. 5, the fluctuating velocity was enhanced by the excitation with low frequency and with the asymmetric mode, thus it is expected to enhance the sinusoidal deformation with the lower excitation. Figure 9 illustrates the velocity distributions along the z-axis for x/w=7 with zigzag excitation without the impinging plate. The position of A, B and C corresponds in the location of the boundary part of the cell as shown in Fig. 8. We take particular note that

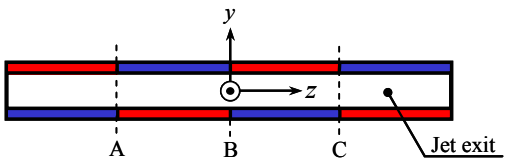

Fig. 8 Zigzag excitation pattern

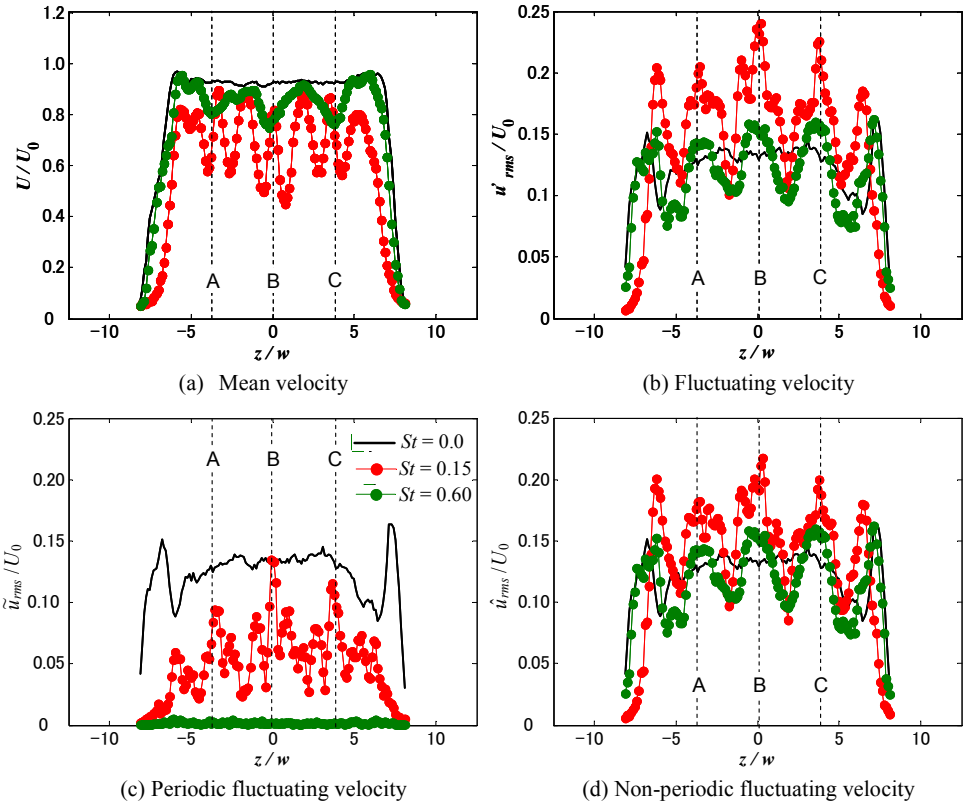

Fig. 9 Velocity distributions along the z-axis for x/w=7 with zigzag excitation

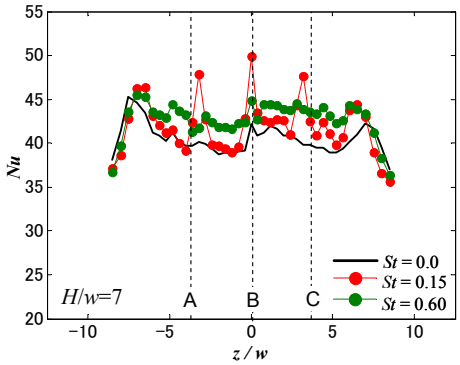

Fig. 10 Nu distribution along the z-axis for H/w=7 with zigzag excitation

the turbulent intensity, u'_{rms}, and the non-periodic velocity, $\hat{u}_{rms}$, had peaks near the parts as shown in Figs. 9(b) and (d). These tendencies were clearly observed for St=0.15. The increase of u'_{rms} is the result of the increase of $\hat{u}_{rms}$.

The heat transfer on the z-axis with the zigzag excitation for H/w=7 is shown in Fig. 10. For the excitation of St=0.15, we find the significant change of the Nu distribution pattern from that for the St=0.0 and 0.60, three peaks appeared near the boundary part. The behavior shown in Fig. 10 could be recognized that the non-periodic velocity component played the most important role in the heat transfer characteristics.

5. Conclusions

The aim of this study is to investigate the effects of acoustic excitation modes of the symmetric excitation and the asymmetric excitation on an impinging jet heat transfer. To clarify the flow field of the excited jet, mean and fluctuating velocity of the free rectangular jet were measured. And the heat transfer characteristics on a flat plate of the impinging jet were measured. The following conclusions can be drawn:

(1) The similar heat transfer characteristics were obtained with the asymmetric and symmetric excitation. The non-periodic velocity component played an important role in promotion of the heat transfer of the impinging jet.

(2) The flow fields of a free jet were strongly affected by the acoustic excitation mode and the frequency.

Acknowledgement

We would like to thank Fuminori Uchiyama of graduate student in Shinshu University for his sincere assistance during the experiment. This work was partly supported by JGC-S SCHOLARSHIP FOUNDATION and Nagano Society for the Promotion of Science.

References

(1)R. Gardon and J.C. Akfirat, The role of turbulence in determining the heat transfer characteristics of impinging jets, *Int. J. Heat Mass Transfer*, Vol.8(1965), pp.1261-1272.

(2)R. Gardon and J.C. Akfirat, Heat transfer characteristics of impinging two-dimensional air jet, *ASME: J. Heat Transfer*, Vol.88(1966), pp.101-108.

(3)K. Oyakawa, M. Yaga, K. Nasu, I. Senaha, S. Matsuda and T. Azama, Impingement heat transfer by jet issuing from cross-shaped nozzle, *Transactions of the Japan Society of Mechanical Engineers. B*, Vol.63, No.607(1997), pp.979-985.

(4)M. Hiwada, S. Tanaka, K. Tanaka and K. Oyakawa, Effect of tabs on impinging heat transfer, *Transactions of the Japan Society of Mechanical Engineers. B*, Vol.66, No.647(2000), pp.1812-1817.

(5)Y. Haneda, Y. Tsuchiya, H.Kurasawa, K. Nakabe and K. Suzuki, Flow field and heat transfer of a two-dimensional impinging jet disturbed by an elastically suspended circular cylinder, *Heat transfer Asian Research*, Vol.30, No.4(2001), pp.313-330.

(6)T. Liu and J.P. Sullivan, Heat transfer and flow structures in an excited circular impinging jet, *Int. J. Heat Mass Transfer*, Vol.39, No.17(1996), pp.3695-3706.

(7)S. D. Hwang, H. H. Cho, Effects of acoustic excitation positions on heat transfer and flow in aximmetric impinging jet: main jet excitation and shear layer excitation, *Int. J. Heat Fluid Flow* Vol.24(2003), pp.199-209.

(8)Edmund A. Singer and A. Ortega, Turbulent heat transfer in a forced and unforced two dimensional air jet impinging on an isoflux surface, *Proc. the ASME Heat Transfer Division*, HTD-Vol.353 Volume 3(1997), pp.55-62.

(9)C. Gau, W.Y. Sheu and C.H. Shen, Impingement cooling flow and heat transfer under acoustic excitations, *J. Heat Transfer*, Vol.119(1997), pp.810-817.

(10)S. Iio, K. Hibino, M. Matsubara and T. Ikeda, Acoustic Control of an Impinging Planer Jet upon a Wedge, *J. Fluid Science and Technology*, Vol.3, No. 2(2008), pp.274-281.

(11)A.K.M.F. Hussain and W.C. Reynolds, The mechanics of an organized wave in turbulent shear flow, *J. Fluid Mech.*, Vol.41, No. 2(1970), pp.241-258.

(12)M. Kumada, T. Nakatogawa and K. Hirata, On the heat and mass transfer of an impinging jet (in Japanese), *Journal of the J.S.M.E.*, Vol.76, No. 655(1973), pp.822-830.